scientific reports

Check for updates

OPEN

Study on the relationship between in-stent neoatherosclerosis and chronic kidney disease: an optical coherence tomography study

Yixuan Gao[1,3], Ning Gu[1,3], Yanna Zhou[2], Yan Wang[1], Ranzun Zhao[1]✉ & Bei Shi[1]✉

The relationship between in-stent neoatherosclerosis (ISNA) and chronic kidney disease (CKD) was investigated among patients exhibiting in-stent restenosis (ISR) after drug-eluting stent (DES) implantation. A total of 220 patients with confirmed in-stent restenosis (ISR) via coronary arteriography between 2020 and 2023 were enrolled. Patients were stratified into three groups based on estimated glomerular filtration rate (eGFR) levels: (1) normal renal function (eGFR ≥ 90 mL/min/1.73 m², n = 80), (2) mild renal impairment (60 ≤ eGFR < 90 mL/min/1.73 m², n = 86), and (3) kidney failure (eGFR < 60 mL/min/1.73 m², n = 54). Baseline clinical characteristics, angiographic parameters, and optical coherence tomography (OCT) data were collected and analyzed across all groups. No significant differences in angiographic characteristics were found between the three groups ($p > 0.05$). Patients with kidney failure demonstrated significantly higher rates of both in-stent neoatherosclerosis (ISNA) (68.5% vs. 46.5% vs. 42.5%; $p < 0.05$) and thin-cap fibroatheroma (TCFA) within ISR lesions (40.7% vs. 22.1% vs. 22.5%; $p < 0.05$) compared to those with mild or normal renal function, respectively. Lower eGFR levels were associated with a higher incidence of ISNA and reduced neointima stability.

Keywords Neoatherosclerosis, In-stent restenosis, Optical coherence tomography, Neutrophil-to-lymphocyte ratio

Coronary heart disease (CHD) is a clinical syndrome caused by coronary artery atherosclerosis (AS), which leads to luminal stenosis or occlusion, resulting in myocardial ischemia, hypoxia, or necrosis[1,2]. Given the progressive nature of atherosclerosis, in-stent restenosis (ISR) may develop following percutaneous coronary intervention (PCI), with in-stent neoatherosclerosis (ISNA) being recognized as the predominant underlying mechanism[3,4].

Chronic kidney disease (CKD) defined as an estimated glomerular filtration rate (eGFR) of less than 60 mL/min/1.73m^2 and/or a urinary albumin to creatinine ratio greater than 30 mg/g (3 mg/mmol)[5]. Previous research had showed that CHD is the leading cause of CKD incidence and mortality[6]. CKD can not only activate inflammatory responses through various pathways to promote the progression of atherosclerosis, but also lead to the occurrence of ISR after PCI[7].

As a main reason for ISR, there is no clear research conclusion on whether there is a correlation between CKD and ISNA. Optical coherence tomography (OCT) is an important technique for clinical observation of ISNA features[8], and OCT based studies had identified CKD as a potential contributing factor to ISNA. Given the elevated clinical risks associated with ISR, elucidating the CKD-ISNA relationship holds significant clinical value for optimizing treatment strategies and prognostic evaluation.

Materials and methods

Study design and patient characteristics

The retrospective observational study included 295 patients diagnosed with ISR by CAG at a single center (Zunyi Medical University Affiliated Hospital) between January 2020 and December 2023. All patients received sirolimus-eluting drug-eluting stents (DES), with no bare metal stent (BMS) implants. Patients with acute and chronic infections, autoimmune diseases, liver failure, malignant tumors, allergic diseases, and the use of anti-

[1]Department of Cardiology, Affiliated Hospital of Zunyi Medical University, No. 149 of Road Dalian, District Huichuan, Zunyi 563000, China. [2]Department of Epidemiology and Health Statistics, Zunyi Medical University, Zunyi 563000, China. [3]Yixuan Gao and Ning Gu have contributed equally to this work. ✉email: kouke80@126.com; shibei2147@163.com

inflammatory or immunosuppressive agents were excluded. Among 295 patients, 75 patients were excluded for following reasons: (1) 20 patients did not undergo OCT due to financial constraints; (2) 11 patients for poor quality of OCT images; (3) 18 patients for insufficient demographic data; and (4) 26 patients with non-first ISR. A total of 220 patients were initially identified for inclusion in the study.

Kidney failure, defined as a baseline estimated glomerular filtration rate (eGFR) <60 mL/min/1.73 m^2, calculated using a modified creatinine-based formula[5]: (1) When the blood creatinine measurement value is ≤62 years for females and ≤80 years for males: females: $144 \times (\text{blood creatinine}/62)^{-0.329} \times 0.993^{age}$; males: $144 \times (\text{blood creatinine}/80)^{-0.411} \times 0.993^{age}$; (2) When the blood creatinine measurement value is >62 years for females and >80 years for males: females: $144 \times (\text{blood creatinine}/62)^{-1.209} \times 0.993^{age}$; males: $144 \times (\text{blood creatinine}/80)^{-1.209} \times 0.993^{age}$.

According to the eGFR levels upon admission, the patients were divided into three groups: group 1 had normal kidney function (eGFR ≥90 ml/min/1.73 m^2), group 2 had mild kidney function (60 ≤eGFR ≤90 ml/min/1.73 m^2), and group 3 had kidney failure (Egfr ≤60 ml/min/1.73 m^2) (including 3 hemodialysis patients) (Fig. 1). The relevant data were collected by experienced doctors using electronic medical record systems in a confidential manner.

The research protocol was approved by the Institutional Review Board of the First Affiliated Hospital of Zunyi Medical University (Approval No. KLL −2019 −323) in accordance with the Declaration of Helsinki (2013 revision). Written informed consent was obtained from all study participants prior to data collection.

Data collection and angiographic characteristics

The baseline data were collected from the medical record system and analyzed. Diagnostic criteria were defined as follows: Hypertension defined as systolic blood pressure ≥140 mmHg and/or diastolic blood pressure ≥90 mmHg, or receiving treatment with antihypertensive drugs. Diabetes defined as fasting venous blood glucose ≥7 mmol/L and/or random venous blood glucose, and 2 h postprandial venous blood glucose ≥11.1 mmol/L, or receiving hypoglycemic drugs. Smoking defined based on whether the patient is currently smoking or has quit smoking within 6 months.

Under stable conditions, 2 mL of fasting peripheral venous blood was collected in the morning after an 8-hour fast. Laboratory measurements included total cholesterol (TC), triglycerides (TG), low-density lipoprotein cholesterol (LDL-C), high-density lipoprotein cholesterol (HDL-C), transaminases, creatinine, eGFR, troponin T, N-terminal pro-B-type natriuretic peptide (NT-proBNP), and routine hematological parameters (white blood cells, hemoglobin, and platelets). The target lesion characteristics of the patients undergoing PCI angiography in the Imaging Core Laboratory of the Zunyi Medical University Affiliated Hospital were collected and analyzed by two independent technicians. Quantitative coronary angiography (QCA) analysis was performed in the core laboratory of the Zunyi Medical University Affiliated Hospital, where Artis VC21C software (Artis VC21C, Siemens AG, Berlin, and Munich) was used by a blinded trained technician to analyze the angiographic images of all patients.

All coronary interventions and perioperative management were conducted in strict accordance with established clinical guidelines, specifically the 2021 American College of Cardiology/American Heart Association/Society for Cardiovascular Angiography and Interventions (ACC/AHA/SCAI) Coronary Artery Revascularization Guidelines (Chinese version) and the 2020 European Society of Cardiology (ESC) Guidelines for the Management of Acute Coronary Syndromes (Chinese version). CAG was performed through the radial or femoral artery using a catheter, and multiple matching CAG images were obtained after injecting nitrate into the coronary artery. Mehran classification was used for ISR classification: type I, focal type (≤ 10 mm), which was subdivided into connected type, marginal type, single focal type, and multi-focal type; type II, diffuse in-stent (> 10 mm, confined to the stenotic stent); type III, proliferative type (> 10 mm, over the edge of the stent); and type IV, complete occlusion[9].

OCT acquisition and assessment

ISR lesions were imaged using OCT catheters and frequency-domain OCT (St. Jude Medical, St. Paul, MN, USA.). The OCT catheter was introduced into distal ISR lesions with a pullback rate of 18 mm/s and rotation rate of 100 frames/s. During pullback, the contrast medium was injected through the guiding catheter at a rate of 3–4 mL/s. Qualitative analyses of OCT images were performed by two experienced physicians who were blinded to clinical and angiographic lesion characteristics. When the two observers had different opinions, they reached a final decision after discussion. To evaluate interobserver differences in OCT diagnosis of ISNA and TCFA, each frame (every 0.1 mm) was analyzed using offline proprietary software (LightLab Imaging Inc., Westford, MA, USA) by two independent cardiologists who had no knowledge of the baseline clinical and angiographic characteristics.

ISNA was defined as the presence of newly formed neointima containing either lipid deposits or calcification. Three distinct morphological patterns of neointimal hyperplasia were characterized using OCT guidance[10]: (1) Homogeneity, with uniform high signal bands and no backscatter patterns; (2) Heterogeneity, mixed signal bands display different backscatter modes; (3) Layered, there are shallow and deep low signal zones around the support beam. On OCT, lipid neointima described as signal difference regions with diffuse boundaries. TCFA defined as a lipid containing neointima with a lipid curvature of 180° and a fiber cap thickness of ≤65 μm[11]. Calcified neointima are clear areas of low backscatter signal difference. Point calcification is defined as a lesion with a length of less than 4 mm and a calcification curvature of 90°. Fibrous neointima is characterized by homogeneous high-signal-intensity areas accompanied by signal attenuation. Thrombotic lesions are identified by three distinct OCT features: (1) luminal protrusion beyond the stent struts, (2) irregular surface contour, and (3) variable signal intensity ranging from normal to hyperintense. The definition of imaging of neointima macrophages is the enrichment of intensity signals in the presence of different or converging areas, where the signal

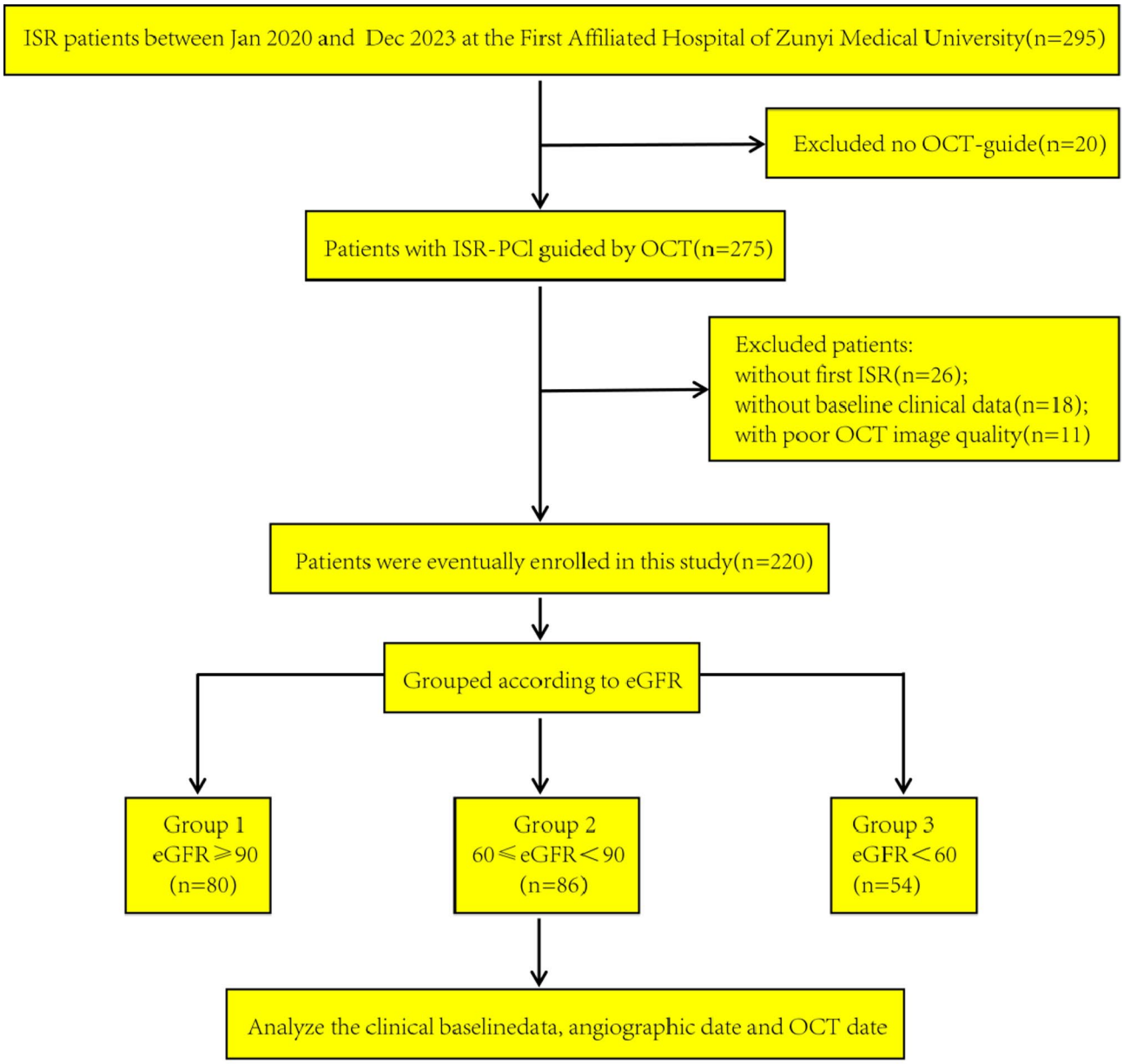

Fig. 1. Enrollment of patients. A total of 220 patients with ISR were included in this study. According to the eGFR levels upon admission, the patients were divided into three groups: group 1 had normal kidney function (eGFR ≥ 90 ml/min/1.73 m^2), group 2 had mild kidney function (60 ≤ eGFR< 90 ml/min/1.73 m^2), and group 3 had kidney failure (eGFR< 60 ml/min/1.73 m^2).

intensity exceeds the background speckle noise. The tissue characterization of restenosis lesions was determined through systematic evaluation. When analyzing cross-sections, lesions were classified as heterogeneous type if any heterogeneous or layered patterns were identified. In the absence of these features, lesions were categorized as homogeneous type. For cases demonstrating both heterogeneous and layered patterns simultaneously, the predominant pattern (constituting the highest proportion) determined the final classification. Additionally, the presence of any of the following features - TCFA, calcified neointima, fibrous neointima, lipid-rich neointima, thrombus, or microvessels - was sufficient to establish the corresponding tissue composition within the lesion.

Figure 2 shows representative OCT images of various ISR vascular morphologies.

Statistical analyses

To address potential confounding effects, all clinically relevant variables were incorporated into a multivariate logistic regression model for statistical adjustment. This approach permitted determination of the independent association between CKD and clinical outcomes. All analyses were conducted using SPSS 29.0 (IBM Corp.,

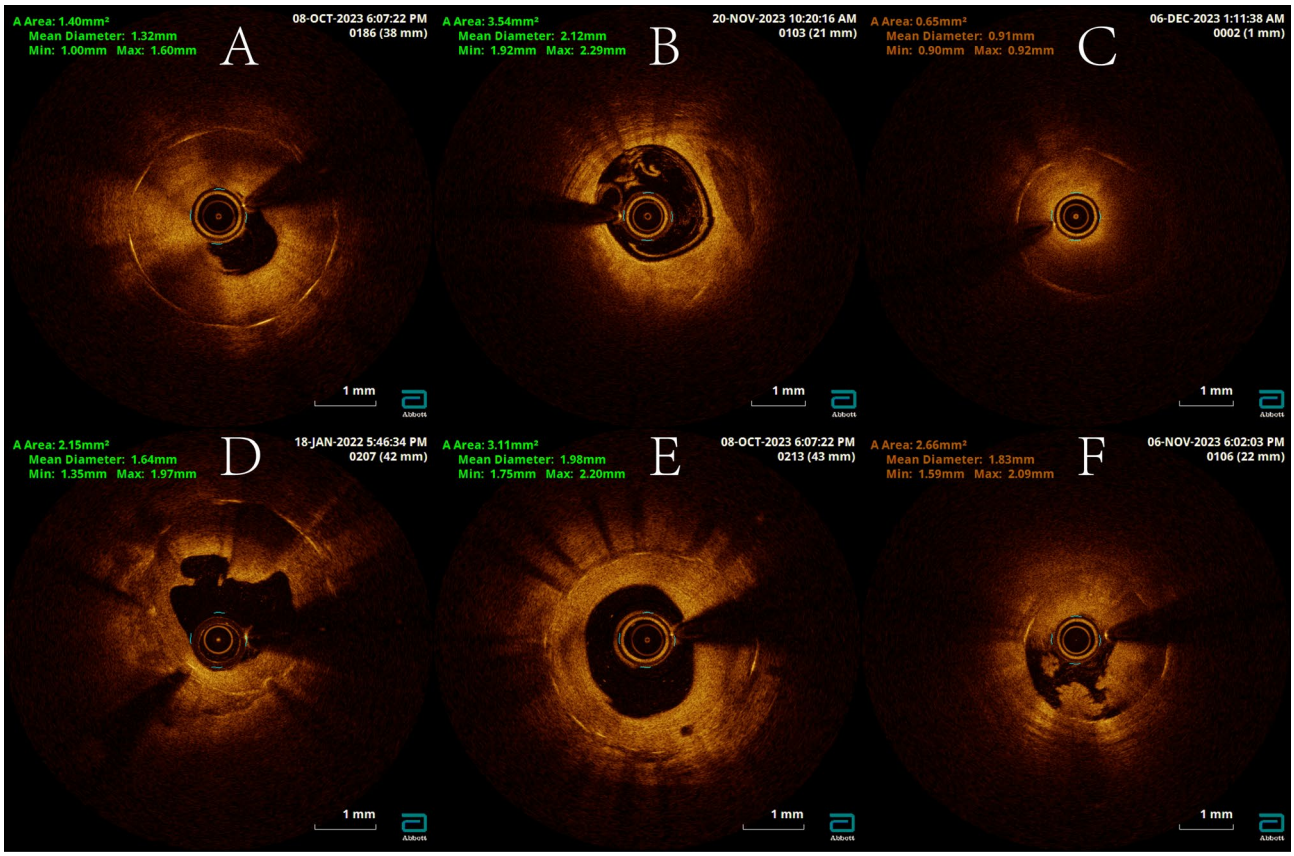

Fig. 2. Representative OCT images of various ISR vascular morphologies. (A) Heterogeneous type; (B) Calcified neointima; (C) Lipid neointima; (D) Plaque rupture; (E) Microchannel; (F) Thrombus.

Armonk, NY, USA, Version 29.0). The statistical description of categorical variables adopts rate or percentage, and statistical inference adopts R×C contingency table chi square test; Performed normality tests on numerical variables, using mean and standard deviation to represent normal distribution, one-way ANOVA for statistical inference, SNK method for pairwise comparison, Kruskal Wallis test for statistical inference, Bonferroni method for pairwise comparison, and testing level $\alpha = 0.05$.

Results

Clinical characteristics

A total of 220 patients with ISR were enrolled in this study, consisting of 177 male and 43 female participants (mean age: 63.45 ± 10.39 years). Mean eGFR levels for each group were as follows: group 1, 105.10 (96.94, 112.18); group 2, 74.68 ± 8.61; and group 3, 48.13 (41.55, 54.08). A significant difference in the baseline was observed between the three groups: the male incidence rate was higher in the mild kidney function group than the normal kidney function group. These significant differences were also reflected in Hemoglobin, ALT, TBIL, Troponin T, and NTPro-BNP (both $p < 0.05$) (Table 1).

Angiographic findings

No significant differences in angiographic characteristics were observed among these patients (Table 2).

OCT analysis of ISR lesions

Significantly higher rates of in-stent neoatherosclerosis (ISNA) (68.5% vs. 46.5% vs. 42.5%; $p = 0.008$) and TCFA (40.7% vs. 22.1% vs. 22.5%; $p = 0.029$) were detected in the kidney failure group compared to the mild and normal renal function groups, respectively. Additionally, lipid-rich neointima was more frequently observed in the kidney failure group (68.5% vs. 50.0% vs. 45.0%; $p = 0.023$). Conversely, a progressive reduction in fibrous neointima incidence was associated with worsening renal function (31.5% vs. 52.3% vs. 52.5%; $p = 0.036$). (Table 3).

Independent predictors of ISNA

Data of 220 patients were used for logistic regression. As shown in Table 4, univariate (OR: 2.945, 95% CI: 1.426–6.083; $p = 0.004$), (OR: 2.368, 95% CI: 1.113–5.038; $p = 0.025$) and multivariate (OR: 5.938, 95% CI: 1.125–31.338; $p = 0.036$), (OR: 5.175, 95% CI: 1.302–20.574; $p = 0.020$) analyses indicated that eGFR level (Group 1 vs. Group 3) was independently associated with the presence of ISNA and TCFA.

	Total ($n=220$)	eGFR ≥ 90 (G1, $n=80$)	60 ≤ eGFR<90 (G2, $n=86$)	eGFR<60 (G3, $n=54$)*	p Value	^{p} Value G1 vs. G2	^{p} Value G1 vs. G3	^{p} Value G2 vs. G3
Age, M ± SD, years	63.45± 10.39	58.40 ± 9.06	63.50 ± 9.85	70.87 ± 8.59	0.000	0.000	0.000	0.000
Gender					0.006	0.001	0.399	0.33
Male, n(%)	177(80.5%)	57(71.3%)	78(90.7%)	42(77.8%)				
Female, n(%)	43(19.5%)	23(28.8%)	8(9.3%)	12(22.2%)				
The incidence type of this time					0.952			
ACS, n(%)		36(37.5%)	37(38.5%)	23(24.0%)				
CCS, n(%)		44(35.5%)	49(39.5%)	31(25.0%)				
Previous MI, n (%)	54(24.5%)	19(23.8%)	23(26.7%)	12(22.2%)	0.815			
Smoker, n(%)	103(46.8%)	37(46.3%)	44(51.2%)	22(40.7%)	0.481			
Hypertension, n(%)	135(61.4%)	42(52.5%)	49(57.0%)	44(81.5%)	0.002	0.563	0.001	0.003
Diabetes, n(%)	59(26.8%)	22(27.5%)	19(22.1%)	18(33.3%)	0.339			
Hyperlipidemia, n(%)	60(27.3%)	22(27.5%)	27(31.4%)	11(20.4%)	0.361			
Laboratory findings								
White blood cells, M(IQR), $\times 10^9$/L	7.06(5.76, 8.68)	7.23(5.76, 8.93)	6.98(5.52, 8.21)	6.99(6.01, 8.44)	0.752			
Hemoglobin, M ± SD, g/L	140.25± 18.17	140.90 ± 18.77	144.14 ± 15.61	133.09 ± 19.27	0.002	0.241	0.013	0.000
Platelet, M ± SD, $\times 10^9$/L	204.78± 72.88	216.20 ± 68.37	198.06 ± 80.77	198.57 ± 64.85	0.214			
Total cholesterol, M ± SD, mmol/L	4.09± 1.47	4.06 ± 1.37	4.05 ± 1.66	4.20 ± 1.30	0.813			
Triglycerides, M(IQR), mmol/L	1.53(1.16, 2.40)	1.64(1.17, 2.38)	1.51(1.13, 2.56)	1.46(1.18, 2.15)	0.975			
HDL-C, M ± SD, mmol/L	1.09± 0.31	1.08 ± 0.28	1.11 ± 0.36	1.09 ± 0.24	0.725			
LDL-C, M ± SD, mmol/L	2.37± 0.94	2.38 ± 0.88	2.31 ± 1.03	2.45 ± 0.91	0.681			
ALT, M(IQR), U/L	26.00(18.00, 36.00)	27.00(19.25, 39.00)	27.00(19.00, 36.00)	20.50(15.00, 32.25)	0.024	0.609	0.012	0.021
TBIL, M(IQR), U/L	12.45(9.33, 17.00)	12.40(8.23, 17.50)	14.25(10.38, 17.88)	11.35(8.20, 13.53)	0.017	0.214	0.144	0.003
Troponin T, M(IQR), ng/L	3.00(1.00, 6.00)	12.36(6.81, 74.66)	12.56(8.74, 23.84)	21.68(12.50, 58.41)	0.003	0.859	0.010	0.001
NTPro-BNP, M(IQR), pg/ml	212.85(92.76, 673.03)	180.55(86.94, 586.68)	193.75(78.46, 415.18)	476.60(120.50, 1735.50)	0.004	0.627	0.005	0.002
Medicine use								
Aspirin, n(%)	207(94.1%)	77(96.3%)	80(93.0%)	50(92.6%)	0.622			
Clopidogrel, n(%)	197(89.5%)	72(90.0%)	78(90.7%)	47(87%)	0.778			
Statin, n(%)	194(88.2%)	73(91.3%)	75(87.2%)	46(85.2%)	0.531			

Table 1. Baseline characteristics. *Including 3 hemodialysis patients. eGFR: estimated glomerular filtration rate; ACS: acute coronary syndrome; CCS: chronic coronary syndrome; MI: myocardial infarct; HDL-C: high-density lipoprotein cholesterol; LDL-C: low-density lipoprotein cholesterol; ALT: Alanine Transaminase; TBIL: total bilirubin; NTPro-BNP: N-terminal pro-B-type natriuretic peptide; M(SD) = mean(stand deviation); M(IQR) = median(interquartile range); p Value<0.05 or the Bonferroni correction for two group comparison was a new significance level of 0.05/3 = 0.017.

Discussion

A significantly higher incidence of ISNA was demonstrated in patients with kidney failure compared to other renal function groups. CKD was consistently identified as an independent predictor for both ISNA development and TCFA formation ($p < 0.01$) through univariate and multivariate regression analyses. These findings suggest that progressive renal function deterioration is associated with ISNA progression, underscoring the necessity for intensified cardiovascular risk monitoring in CKD patients receiving percutaneous coronary intervention. Based on OCT and histopathological evidence, ISNA has been established as the predominant biological mechanism underlying ISR. This pathological process is characterized by an exaggerated healing response triggered by arterial wall injury during stent deployment[12,13]. The distribution of neointima tissue hyperplasia can be focal or diffuse along the length of the stent. The condition is primarily caused by local inflammation resulting from mechanical damage to the endometrium/media, leading to invasive neointima hyperplasia or proliferation composed of smooth muscle cells and extracellular matrix[14,15]. ISNA is an important mechanism of stent failure that is increasingly recognized in contemporary DES. It is characterized by the accumulation of lipid foam macrophages and the formation of necrotic cores in the stent segment[16]. The injury of balloon inflation and stent deployment to blood vessels stimulates the formation of new intima, which leads to the proliferation and migration of vascular smooth muscle cells, macrophages and extracellular matrix[17]. This process activates the coagulation cascade and inflammatory response, which together slow down endothelial healing. Endothelial denudation following DES implantation permits early LDL-C infiltration into the arterial wall, ultimately leading to atherosclerotic plaque formation. Furthermore, neointimal hyperplasia has been attributed to hypersensitivity reactions against metallic and/or polymeric components in early-generation DES platforms[18,19].

Previous researches already reported that CKD positively correlated with AS and ISR, and as kidney function gradually deteriorates, the incidence of ISR and AS also increases[20]. The association between CKD and lipid

	Total ($n = 220$)	eGFR ≥ 90 (G1, $n = 80$)	60 ≤ eGFR<90 (G2, $n = 86$)	eGFR<60 (G3, $n = 54$)	^{p} Value
Time since stent implantation, M(IQR), years	3.00(1.00, 6.00)	3.00(1.00, 6.00)	2.50(1.00, 5.00)	4.00(1.00, 6.50)	0.354
Culprit vessel					
Left anterior descending, n(%)	138(62.7%)	48(60.0%)	54(62.8%)	36(66.7%)	0.736
Circumflex, n(%)	20(9.1%)	10(12.5%)	6(7.0%)	4(7.4%)	0.412
Right, n(%)	60(27.3%)	22(27.5%)	24(27.9%)	14(25.9%)	0.966
Other, n(%)	2(0.9%)	0(0.0%)	2(2.3%)	0(0.0%)	0.342
Lesion Characteristics					
Bifurcation(>1.5 mm), n(%)	50(22.7%)	15(18.8%)	18(20.9%)	17(31.5%)	0.198
Ostial location, n(%)	15(6.8%)	7(8.8%)	5(5.8%)	3(5.6%)	0.690
In-stent restenosis pattern*					
Type I, n(%)	59(26.8%)	17(21.3%)	26(30.2%)	16(29.6%)	0.369
Type II, n(%)	54(24.5%)	22(27.5%)	21(24.4%)	11(20.4%)	0.642
Type III, n(%)	53(24.1%)	20(25.0%)	17(19.8%)	16(29.6%)	0.402
Type IV, n(%)	54(24.5%)	21(26.3%)	22(25.6%)	11(20.4%)	0.710

Table 2. Angiography characteristics. eGFR: estimated glomerular filtration rate; M(IQR) = median(interquartile range);*p* Value < 0.05 or the Bonferroni correction for two group comparison was a new significance level of 0.05/3= 0.017. *Instent restenosis pattern was defined as per Mehran's classification.

	Total ($n = 220$)	eGFR ≥ 90 (G1, $n = 80$)	60 ≤ eGFR<90 (G2, $n = 86$)	eGFR<60 (G3, $n = 54$)	^{p} Value	^{p} Value G1 vs. G2	^{p} Value G1 vs. G3	^{p} Value G2 vs. G3
Quantitative assessment								
Distal reference lumen area, M ± SD, mm^2	5.01± 2.09	4.80 ± 2.15	5.38 ± 2.16	4.71 ± 1.84	0.103			
Distal reference lumen diameter, M ± SD, mm	2.45± 0.58	2.37 ± 0.57	2.57 ± 0.63	2.39 ± 0.47	0.061			
Proximal reference lumen area, M(IQR), mm^2	8.15(6.71, 9.47)	8.28(6.28, 9.79)	8.45(6.87, 9.44)	7.25(6.46, 9.02)	0.109			
Proximal reference lumen diameter, M(IQR), mm	3.23(2.93, 3.47)	3.25(2.85, 3.53)	3.26(2.96, 3.46)	3.06(2.91, 3.43)	0.256			
Minimum lumen area, M ± SD, mm^2	1.83± 0.76	1.80 ± 0.80	1.95 ± 0.78	1.68 ± 0.62	0.117			
Minimum lumen diameter, M(IQR), mm	1.42(1.25, 1.67)	1.42(1.24, 1.70)	1.46(1.30, 1.70)	1.37(1.25, 1.57)	0.217			
NIH%, M ± SD, %	0.72± 0.11	0.70 ± 0.13	0.73 ± 0.09	0.72 ± 0.10	0.098			
Qualitative assessment								
ISNA, n(%)	111(50.5%)	34(42.5%)	40(46.5%)	37(68.5%)	0.008	0.603	0.003	0.011
Restenostic tissue structure					0.149			
Homogeneous, n(%)	94(42.7%)	36(45.0%)	41(47.7%)	17(31.5%)				
Heterogeneous, n(%)	102(46.4%)	33(41.3%)	36(41.9%)	33(61.1%)				
Layered, n(%)	24(10.9%)	11(13.8%)	9(10.5%)	4(7.4%)				
TCFA, n(%)	59(26.8%)	18(22.5%)	19(22.1%)	22(40.7%)	0.029	0.950	0.024	0.018
Calcific neointima, n(%)	17(7.7%)	10(12.5%)	2(2.3%)	5(9.3%)	0.044	0.011	0.559	0.152
Fibrous neointima, n(%)	104(47.3%)	42(52.5%)	45(52.3%)	17(31.5%)	0.028	0.982	0.016	0.016
Lipid neointima, n(%)	116(52.7%)	36(45.0%)	43(50.0%)	37(68.5%)	0.023	0.519	0.007	0.031
Thrombus, n(%)	52(23.6%)	23(28.8%)	19(22.1%)	10(18.5%)	0.358			
Microvessels, n(%)	121(55.0%)	44(55.0%)	48(55.8%)	29(53.7%)	0.971			

Table 3. ISR characteristics evaluated by optical coherence tomography. M(SD) = mean(stand deviation); M(IQR) = median(interquartile range); NIH: neointimal hyperplasia; ISNA: in-stent neoatherosclerosis; TCFA: thin-cap fibroatheroma; *p* Value<0.05 or the Bonferroni correction for two group comparison was a new significance level of 0.05/3 = 0.017.

plaque progression was first documented by Sugiyama et al., with subsequent studies demonstrating that CKD advancement may accelerate the acceleration of atherosclerotic changes[21]. A significant association between CKD and elevated risks of myocardial infarction and mortality was demonstrated by Osorio Gomes et al.[22]. Significantly greater intimal hyperplasia progression and higher restenosis recurrence rates were observed in non-hemodialysis-dependent CKD patients compared to those with normal renal function during post-PCI follow-up, as demonstrated by Aoyama et al.[23].

No comparative studies examining the association between CKD and neoatherosclerosis following ISR have been previously reported. A significant promotive effect of CKD on ISNA progression was demonstrated, with ISNA incidence showing a graded increase corresponding to declining renal function. This association may be

	Group 1	Group 2		Group 3		
	OR	OR (95%CI)	*p* Value	OR (95%CI)	*p* Value	*p* Trend
ISNA						
Model 1	1.000	1.176 (0.637–2.172)	0.603	2.945 (1.426–6.083)	0.004	
Model 2	1.000	1.043 (0.544–2.001)	0.898	2.575 (1.140–5.818)	0.023	
Model 3	1.000	1.054 (0.548–2.026)	0.875	2.735 (1.184–6.317)	0.018	
Model 4	1.000	3.791 (0.995–14.440)	0.051	5.938 (1.125–31.338)	0.036	
TCFA						
Model 1	1.000	0.977 (0.470–2.030)	0.950	2.368 (1.113–5.038)	0.025	
Model 2	1.000	0.818 (0.379–1.767)	0.610	1.888 (0.797–4.474)	0.149	
Model 3	1.000	0.826 (0.382–1.787)	0.627	2.060 (0.857–4.950)	0.106	
Model 4	1.000	1.827 (0.606–5.504)	0.284	5.175 (1.302–20.574)	0.020	

Table 4. Univariate and multivariate logistic regression models between CKD with ISNA and TCFA incidence. ISNA: in-stent neoatherosclerosis; TCFA: thin-cap fibroatheroma; Model 1 was adjusted for none. Model 2 was adjusted for age and gender. Model 3 was further adjusted for hypertension and atrial fibrillation on the basis of model 2. Model 4 was further adjusted for hemoglobin, ALT, NTPro-BNP and Troponin T on the basis of model 3; CI: Confidence interval, OR: Odds ratio; *p* Value<0.05 or the Bonferroni correction for two group comparison was a new significance level of 0.05/3 = 0.017.

explained by two pathophysiological mechanisms: (1) atherosclerotic acceleration induced by CKD, and (2) dysregulated neointimal progression status. As research data showed, CKD is clearly associated with age, gender, and history of hypertension. As age increases, the degree of CKD becomes more severe, and the overall trend of CKD degree in males is higher than that in females. The CKD degree in the population with hypertension becomes more severe, and age, gender, and history of hypertension are all clear reasons for the formation of AS. Male kidney function often declines faster than females, which reinforces the importance of gender in CKD outcomes[24].

The clear relationship between CKD and high-sensitivity troponin T, NTPro-BNP also indicates that CKD patients can worsen heart damage and increase disease risk through various pathways, such as coronary artery disease and increased cardiac load. The association between CKD and coronary artery disease has been extensively documented in contemporary literature, with numerous studies establishing consistent pathophysiological links across all CKD stages. In summary, CKD can promote the progression of AS through six major pathways, such as reducing the metabolism of inflammatory factors such as interleukin 1,6[25], TNF[26], C-reactive protein[27], TGF-β[28], etc., promoting the formation of chronic inflammation and oxidative stress response[29,30]; Damage to vascular endothelial function[31,32]; Promote the formation of vascular calcification[33,34]; The involvement of uremic toxins[35,36]; Immune dysfunction[37,38]; Epigenetic effects[39].

While no statistically significant differences in stent/vascular lesion characteristics were detected by CAG across CKD stages, OCT imaging revealed significant associations between CKD severity and specific neointimal patterns: (1) lipid-rich neointima, (2) calcified neointima, (3) fibrotic neointima, and (4) TCFA. Progressive renal dysfunction was correlated with exacerbated neointimal advancement and calcification severity, resulting in measurable reductions in stent lumen area and elevated hemodynamic risk profile[40,41].

From the prediction results, CKD can predict the occurrence of ISNA and TCFA. As kidney function deteriorates, the probability of ISNA and TCFA occurrence increases linearly, and the difference between the normal kidney function group and the kidney failure group is greater, indicating a clear correlation between the two.

During clinical practice, many patients with CHD may have CKD status during their course of illness, either simultaneously or sequentially. While treating CHD, more attention should be to paid to treat CKD, because cardiovascular doctors tend to focus more on the heart status and easily overlook the treatment of kidney disease. These findings underscore the necessity for nephrology consultation in post-PCI management, particularly for stent-implanted patients, with multidisciplinary collaboration representing an emerging standard of care. Furthermore, the demonstrated predictive relationships warrant intensified cardiovascular risk stratification in CKD populations, enabling earlier identification of high-risk profiles and subsequent prognostic optimization.

Limitations

The current research had certain limitations. First, it's a single center, retrospective study with a relatively limited sample size, which may introduce potential bias. Larger population size is needed to prove long term outcomes. Second, the diagnosis of CKD is based on a comprehensive assessment of past medical history and kidney function test results upon admission, which may introduce potential selection bias, and the data obtained from this study may not represent a broader patient population. Third, it's a cross-sectional study and lacks follow-up data and prognostic analysis. Fourth, there is a lack of histological validation of the characteristics of neointima tissue. Although OCT is the preferred intravascular imaging method for diagnosing ISNA, it has its own

limitations and may not accurately evaluate qualitative neointima features. The arterial sclerosis caused by CKD is largely related to the involvement of inflammatory factors. The specific factors that play a more important role in the progression of AS in CKD require further basic research to be clearly identified. The present analysis was limited to the documentation of clinical associations and preliminary mechanistic interpretations derived from available biomarker indicators.

Conclusion

A significant positive association was observed between CKD severity and ISNA incidence, with progressive renal dysfunction correlating with elevated ISNA prevalence. This relationship may be mediated through CKD-induced systemic inflammation, which has been demonstrated to potentiate both atherosclerotic progression and pathological neointimal formation.

Data availability

Due to privacy and ethical constraints, the datasets generated and analysed in this study are not publicly available but can be obtained from the corresponding author.

Received: 12 November 2024; Accepted: 2 June 2025
Published online: 01 July 2025

References

1. Doenst, T. et al. The treatment of coronary artery disease. *Dtsch. Arztebl Int.* **119** (42), 716–723 (2022).
2. China, T. & Hu, S. S. Report on cardiovascular health and diseases in China 2021: an updated summary. *J Geriatr Cardiol* **20**(6), 399–430 (2023).
3. Sakai, R. et al. Impact of triglyceride-rich lipoproteins on early in-stent neoatherosclerosis formation in patients undergoing Statin treatment. *J. Clin. Lipidol.* **17** (2), 281–290 (2023).
4. Giustino, G. et al. Coronary In-Stent restenosis: JACC State-of-the-Art review. *J. Am. Coll. Cardiol.* **80** (4), 348–372 (2022).
5. Lamprea-Montealegre, J. A., Shlipak, M. G. & Estrella, M. M. Chronic kidney disease detection, staging and treatment in cardiovascular disease prevention. *Heart* **107** (16), 1282–1288 (2021).
6. Lee, H. F. et al. Impact of chronic kidney disease on long-term outcomes for coronary in-stent restenosis after drug-coated balloon angioplasty. *J. Cardiol.* **78** (6), 564–570 (2021).
7. Dai, Z. & Zhang, X. Pathophysiology and Clinical Impacts of Chronic Kidney Disease on Coronary Artery Calcification. *J. Cardiovasc. Dev. Dis.* **10**(5), (2023).
8. Araki, M. et al. Optical coherence tomography in coronary atherosclerosis assessment and intervention. *Nat. Rev. Cardiol.* **19** (10), 684–703 (2022).
9. Takahashi, T. et al. Coronary physiologic assessment based on angiography and intracoronary imaging. *J. Cardiol.* **79** (1), 71–78 (2022).
10. Gonzalo, N. et al. Optical coherence tomography patterns of stent restenosis. *Am. Heart J.* **158** (2), 284–293 (2009).
11. Nakamura, D. et al. Different neoatherosclerosis patterns in Drug-Eluting- and Bare-Metal stent Restenosis - optical coherence tomography study. *Circ. J.* **83** (2), 313–319 (2019).
12. Yu, H. et al. Prevalence, morphology, and predictors of Intra-Stent plaque rupture in patients with acute coronary syndrome: an optical coherence tomography study. *Clin. Appl. Thromb. Hemost.* **28**, 10760296221146742 (2022).
13. Chen, Z. et al. Prevalence and impact of neoatherosclerosis on clinical outcomes after percutaneous treatment of Second-Generation Drug-Eluting stent restenosis. *Circ. Cardiovasc. Interv*. **15** (9), e011693 (2022).
14. Fahed, A. C. & Jang, I. K. Plaque erosion and acute coronary syndromes: phenotype, molecular characteristics and future directions. *Nat. Rev. Cardiol.* **18** (10), 724–734 (2021).
15. Meng, L. et al. Incidence and predictors of neoatherosclerosis in patients with early In-Stent restenosis determined using optical coherence tomography. *Int. Heart J.* **61** (5), 872–878 (2020).
16. Yuan, X. et al. Lipoprotein (a) is related to In-Stent neoatherosclerosis incidence rate and plaque vulnerability: optical coherence tomography study. *Int. J. Cardiovasc. Imaging*. **39** (2), 275–284 (2023).
17. Abouelnour, A. & Gori, T. Intravascular imaging in coronary stent restenosis: prevention, characterization, and management. *Front. Cardiovasc. Med.* **9**, 843734 (2022).
18. Lee, J. et al. Neoatherosclerosis prediction using plaque markers in intravascular optical coherence tomography images. *Front. Cardiovasc. Med.* **9**, 1079046 (2022).
19. Nakamura, D. et al. Predictors and outcomes of neoatherosclerosis in patients with in-stent restenosis. *Eurointervention* **17** (6), 489– (2021).
20. Jonas, M. et al. Cardiovascular outcomes following percutaneous coronary intervention with drug-eluting balloons in chronic kidney disease: a retrospective analysis. *BMC Nephrol.* **21** (1), 445 (2020).
21. Sugiyama, T. et al. Impact of chronic kidney disease stages on atherosclerotic plaque components on optical coherence tomography in patients with coronary artery disease. *Cardiovasc. Interv Ther.* **32** (3), 216–224 (2017).
22. Osorio Gomes, V. et al. Impact of chronic kidney disease on the efficacy of drug-eluting stents: long-term follow-up study. *Arq. Bras. Cardiol.* **96** (5), 346–351 (2011).
23. Aoyama, Y. et al. Impact of chronic kidney disease on a re-percutaneous coronary intervention for sirolimus-eluting stent restenosis. *Coron. Artery Dis.* **23** (8), 528–532 (2012).
24. Yi, T. W. & Levin, A. Sex, gender, and cardiovascular disease in chronic kidney disease. *Semin Nephrol.* **42** (2), 197–207 (2022).
25. Hassan, M. O. et al. Interleukin-6 gene polymorhisms and interleukin-6 levels are associated with atherosclerosis in CKD patients. *Clin. Nephrol.* **93** (1), 82–86 (2020).
26. Lee, S. J., Lee, I. K. & Jeon, J. H. Vascular calcification-new insights into its mechanism. *Int. J. Mol. Sci.* **21**(8), (2020).
27. Xiang, X. et al. Coronary artery calcification in patients with advanced chronic kidney disease. *BMC Cardiovasc. Disord.* **22** (1), 453 (2022).
28. Kaesler, N. et al. Cardiac remodeling in chronic kidney disease. *Toxins (Basel)*, **12**(3). (2020).
29. Olivier, V. et al. Factors of microinflammation in non-diabetic chronic kidney disease: a pilot study. *BMC Nephrol.* **21** (1), 141 (2020).
30. Lai, J. et al. Research progress on the relationship between coronary artery calcification and chronic renal failure. *Chin. Med. J. (Engl).* **131** (5), 608–614 (2018).
31. Zietzer, A. et al. MicroRNA-mediated vascular intercellular communication is altered in chronic kidney disease. *Cardiovasc. Res.* **118** (1), 316–333 (2022).
32. Diaz-Ricart, M. et al. Endothelial damage, inflammation and immunity in chronic kidney disease. *Toxins (Basel)*, **12**(6). (2020).

33. Yun, H. R. et al. Coronary artery calcification score and the progression of chronic kidney disease. *J. Am. Soc. Nephrol.* **33** (8), 1590–1601 (2022).
34. Dusing, P. et al. Vascular pathologies in chronic kidney disease: pathophysiological mechanisms and novel therapeutic approaches. *J. Mol. Med. (Berl).* **99** (3), 335–348 (2021).
35. Dai, L. et al. Early vascular ageing in chronic kidney disease: impact of inflammation, vitamin K, senescence and genomic damage. *Nephrol. Dial Transpl.* **35** (Suppl 2), ii31–ii37 (2020).
36. Lano, G., Burtey, S. & Sallee, M. Indoxyl sulfate, a uremic endotheliotoxin. *Toxins (Basel)*, **12**(4). (2020).
37. van der Poll, T. & Parker, R. I. Platelet activation and endothelial cell dysfunction. *Crit. Care Clin.* **36** (2), 233–253 (2020).
38. Jerez-Dolz, D. et al. Internalization of microparticles by platelets is partially mediated by toll-like receptor 4 and enhances platelet thrombogenicity. *Atherosclerosis* **294**, 17–24 (2020).
39. Piko, N. et al. Atherosclerosis and epigenetic modifications in chronic kidney disease. *Nephron* **147** (11), 655–659 (2023).
40. Tan, K. C. B. et al. Carbamylated lipoproteins and progression of diabetic kidney disease. *Clin. J. Am. Soc. Nephrol.* **15** (3), 359–366 (2020).
41. Sugita, H. et al. Factors associated with coronary In-Stent restenosis after Drug-Eluting stent implantation in patients on chronic Hemodialysis. *Blood Purif.* **51** (4), 383–389 (2022).

Author contributions

Y.G. and N.G. conducted the data analysis statistics and wrote the manuscript. Y.Z. and Y.W. conducted the collection of data. R.Z. and B.S. reviewed and edited the manuscript before submission. All authors read and approved the final manuscript.

Funding

This work was supported by a scientific research project from the National Natural Science Foundation of China (Grant Nos. 82200316,82160057 and 82060061). Innovation Team of Guizhou Provincial Higher Education Institutions (Basic and Clinical Transformation Research on Myocardial and Vascular Injury Repair) (Guizhou Education and Technology [2023]074). The Guizhou Provincial Basic Research Program (Natural Science) (Qiankehe Foundation-ZK [2021]353,ZK[2022] 628,ZK[2023]567).This study was also supported by the Science and Technology Collaboration Achievements - LC[2023]016.

Declarations

Competing interests

The authors declare no competing interests.

Additional information

Correspondence and requests for materials should be addressed to R.Z. or B.S.